Applications of Computational Modeling in Cardiac Surgery

Lik Chuan Lee, Martin Genet, Alan B. Dang, Liang Ge, Julius M. Guccione, Mark B. Ratcliffe

Applications of Computational Modeling in Cardiac Surgery

Lik Chuan Lee, PhD [1,2,3,4], Martin Genet, PhD [1,2,3,5], Alan B. Dang, MD [1,2,3,4], Liang Ge, PhD [1,2,3,4], Julius M. Guccione, PhD [1,2,3,4] and Mark B. Ratcliffe, MD [1,2,3,4].

From the Departments of Surgery[1], Bioengineering[2], and Medicine[3] from the University of California, San Francisco, California and the Veterans Affairs Medical Center, San Francisco, California[4], Marie-Curie postdoctoral fellow[5]

Running Head: Applications of Computational Modeling in Cardiac Surgery

Text Word Count: 5535 words.

Abstract Word Count: 127 words

Number of Figures: 5

Number of Tables: 0

Corresponding Author: Mark B. Ratcliffe, MD, Division of Surgical Services (112), San Francisco Veterans Affairs Medical Center, 4150 Clement Street, San Francisco, California 94121. Telephone: (415) 221-4810. FAX: (415) 750-2181. E-mail: Mark.Ratcliffe@va.gov

Abstract

Computational modeling has pervaded in many areas of science and engineering, but it is only fairly recently that advances in experimental techniques and medical imaging have allowed this tool to be applied in cardiac surgery. Despite its infancy in cardiac surgery, computational modeling has been useful in elucidating and predicting the effects of various heart diseases and clinical interventions. In this review, we used various examples to demonstrate the capabilities of computational cardiac modeling. Specifically, we demonstrate its ability to simulate surgery, predict myofiber stress and pump function, and quantify changes to myocardial material properties. In addition, some of the issues that would need to be resolved in order for computational modeling to play a greater role in cardiac surgery are also laid out in this review.

Keywords: Computational modeling, Finite element method, Medical devices, Myocardial infarction.

1. Introduction

Computational modeling (or computer simulation, mathematical modeling) has pervaded in many areas of science and engineering. With the continuing increase in computing power, mathematical modeling has become an indispensable tool in scientific research and engineering product development of many industries, such as the automotive and aerospace industries.

Among the many benefits associated with the use of computational modeling, two key benefits stand out. First, computational modeling is versatile and can be used to probe the many "what if" scenarios without incurring the typical high costs associated with constructing new experiments. For example, once a computational model is created, the model can be used to quantify the relative contribution of each mechanism in the human heart towards some observed phenomenon. Second, computational modeling is particularly useful in quantifying results that are difficult or impossible to measure in experiments, e.g. when the placement of accelerometers to measure vibrational response is difficult or impossible at certain locations in an automobile or aircraft.

Compared to these engineering areas, computational modeling of the heart is still at its infancy. This is primarily so because living tissues, unlike engineering materials, have highly complex microstructure and can have behavior that evolves with time (i.e. it can remodel and grow) [1,2]. As a consequence, and due in part to the inherent difficulties in performing experiments on living tissues, constitutive relationships of the myocardium such as stress-strain relationship are difficult to construct. Nevertheless, computational models of the heart have continued to improve tremendously over the past few decades. To get a glimpse of this improvement, all one needs to do is to compare early computational models of the heart to the latest models. For example, one of the earliest computational model of the left ventricle (LV) was formulated based on small deformation theory with the assumption that the myocardium is isotropic and has a linear elastic stress-strain relationship [3]. By comparison, a recent biventricular model was not only formulated based on large deformation theory but also takes into account the microstructural arrangement of fiber in the myocardium (i.e. accounting for anisotropy[1]), nonlinearity of the myocardial stress-strain relationship and excitation-contraction coupling of the myocardial tissues [4]. For a more detailed history of the computational modeling in cardiovascular mechanics, refer to Guccione et al. [5].

With these improvements, computational modeling is increasingly applied to problems in cardiac surgery over the past decade. These applications range from elucidating the effects of various heart diseases to predicting the effects of clinical interventions. The goal of this article is to demonstrate the specific capabilities of computational cardiac modeling using various examples, specifically, its ability to simulate

[1] Anisotropy, as opposed to isotropy where the material response is independent of the direction, implies that the material response is direction-dependent.

surgery, predict myofiber stress and pump function, and quantify changes to myocardial material properties. Due to space constraint, we shall confine this review to applications involving only computational modeling of cardiac mechanics, while neglecting the discussion of computational modeling of other equally important sub-fields in cardiac surgery such as electrophysiology. Also, as an aside, most existing computational models of the heart are not truly mechanistic models, which are solely derived from the most basic law of physics. These models are largely phenomenological, and are constructed based on experimental observations (e.g. through mechanical testing of cardiac tissues).

2. Computational Modeling

2.1 Computational Cardiac Mechanics

Broadly speaking, computational cardiac mechanics is at the intersection of three scientific domains, namely, continuum mechanics, materials science and numerical methods (Fig. 1a). Continuum mechanics is the basic reference framework of mechanical engineering that was developed with the expansion of engineering. For a description of the history of continuum mechanics, refer to Fung [6]. Continuum mechanics is based upon a bold hypothesis: that matter is continuous. This is, of course, not exactly true. However, at scales above the nanometer, this hypothesis is very realistic and provides an adequate description of the deformation of matter through the equilibrium equations that all matters must satisfied. These equilibrium equations are derived from basic conservation laws, which are namely, the conservation of mass, momentum, energy. They are general and apply to all types of materials, be it ceramics, metals or living tissues.

The material or constitutive law differentiates between materials. Developed for each specific material, this law describes how much force is developed when the material is stretched or strained, or the converse. Simply put, the constitutive law describes the material mechanical behavior. Many different constitutive laws have been formulated for cardiac tissues and they all share the key features of having a nonlinear and anisotropic stress-strain relationship, and having the ability to contract in the muscle fiber direction when stimulated. Due to its simplicity, we have mostly used the constitutive laws formulated by Guccione et al. [7, 8] in our models. These laws have been extensively validated in large animal studies.

Combining the equations from continuum mechanics and constitutive law leads to a set of (coupled partial differential) equations. The displacement/strain/stress at every material point within the heart wall and every time point during the cardiac cycle can be found once these coupled equations are solved. However, these equations usually cannot be solved analytically for real heart geometries and loading; and its solution can only be found for a few specialized cases with idealized heart geometry. Therefore, one is forced to look for approximated solutions of this set of equations.

Numerical methods, which forms the last pillar of computational cardiac mechanics, is often used to approximate systems of differential equations. Although many numerical methods can be used to approximate systems of equations in cardiac mechanics, the most widely used method is the finite element (FE) method. Its popularity is largely due to its versatility, performance and solid theoretical foundation (e.g. proof of convergence, error control, etc.). The main idea behind the FE method (and in all numerical methods) is to split the original continuous problem into a discrete one, a process typically known as "discretization". To achieve that, the FE method split the material domain into many subparts called elements whose vertices are called nodes. Together, the nodes and elements form the mesh that is typically known as an FE mesh (Fig. 1b). In the FE method, the approximate solution is expressed as the weighted sum of a finite number of known functions called shape functions. One shape function is associated with each node and the shape function is usually chosen to be linear within each element; though higher order shape functions (such as quadratic shape functions) can also be used. The weights associated with each shape function are derived to obtain the best possible approximation with that particular set of shape functions. The result is a large system of algebraic equations that can be solved most efficiently with computers.[2]

For the interested readers, we have provided a more simplified description of the FE method in relation to the three abovementioned domains in the Appendix.

2.2 Finite element over Laplace's law to calculate ventricular wall stress

Given the popularity of using Laplace's law to calculate ventricular wall stress among clinicians, it is worthwhile to examine some of the key merits of using the FE method over Laplace's law. Certainly, there must exist some very good reasons why the FE method should be preferred over Laplace's law, especially since the FE method is much more complicated and requires significantly more effort than Laplace's law. For a comprehensive review of the analytical and numerical methods used to calculate ventricular wall stresses, refer to Yin [9].

The key indisputable advantage of FE method over Laplace's law is its versatility. In particular, once the stress-strain relationship is validated, the FE method can be used to calculate regional stresses in any arbitrary geometry and under any arbitrary load(s). In comparison, Laplace's law was formulated based on the restrictive assumption of a thin ventricular wall, where the law (in its simplest form) states that the ventricular wall stress is directly proportional to the ventricular cavity pressure and endocardial radius of curvature, and is inversely proportional to the ventricular wall thickness. As a consequence, stress is

[2] When the system of algebraic equations is nonlinear, these equations are typically turned into a series of linear equations or "linearized" or before solving with a computer. The most commonly used method for this "linearization" is the Newton-Raphson method

uniform across the ventricular wall. Laplace's law therefore can only calculate average stresses across the ventricular wall. Because the ventricular wall is inhomogeneous with muscle fiber orientation varying across the wall thickness [10], the use of Laplace's law to quantify forces acting or generated by the muscle fiber (i.e. myofiber stress) is bound to be erroneous. To illustrate this, Zhang et al. [11] recently compared stresses in an infarcted sheep LV calculated from the FE method to that calculated from Laplace's law. Not only did they find that Laplace's law severely underestimated the average myofiber stress in both remote (by 64%) and borderzone (BZ) region (by 35%) at end-systole (ES) when compared to the FE method, they also found a significant disparity in stress predicted by the two methods when used to study the effects of Dor procedure. Being more general and without any restrictive assumptions other than the validity of the material constitutive law, the FE method is clearly more accurate. Hence, caution should be exercised when using Laplace's law to quantify myofiber stress.

The other advantage of FE method is that it has a more extensive predictive capability than Laplace's law, whose only utility is in ventricular stress estimation. Not only does it predict regional stresses more accurately, it can also be used to predict material deformation that is impossible to do so using Laplace's law. This predictive capability enables other metrics of cardiac function, such as stroke volume and regional myocardial strains, to be quantified. Moreover, clinical interventions and the effects due to the progression of heart diseases can also be simulated realistically using the FE method. All these capabilities make the FE method a potentially powerful tool with high clinical value.

3. Application in Cardiac Surgery

In his 1981 review paper on ventricular wall stress, Yin [9] aptly stated: "*Our ability to optimally utilize this powerful [FE] method of analysis is also currently limited by our inability to define very accurately the moment-to-moment three-dimensional geometry of the ventricle and our lack of data relative to the regional constitutive relations of myocardial tissue. Unfortunately, until all of these problems are resolved satisfactorily, this powerful tool, which has the potential for providing otherwise unobtainable insight into regional myocardial mechanics, remains of qualitative use and is of limited utility for clinical applications.*" Some thirty years later, with the advancement in experimental techniques to quantify myocardial material response, and imaging techniques that not only makes it possible to construct accurate patient-specific ventricular geometry but is also capable of measuring *in vivo* myocardial deformation, computational cardiac modeling has become more applicable for clinical use. Indeed, computational cardiac modeling has increasingly been used to elucidate the effects of various heart diseases and clinical interventions. We now demonstrate four specific capabilities of computational cardiac modeling using examples.

3.1 Prediction of myofiber stress

Since elevated myofiber stress is widely believed to be responsible for adverse cardiac remodeling [12], knowledge of the *in vivo* regional myofiber stress may shed considerable light on the prognosis of heart diseases in patients and/or the efficacy of any particular treatment received by the patients. To these ends, Laplace's law is often used to estimate ventricular myofiber stress. However, as mentioned earlier, the accuracy of Laplace's law can suffer due to the restrictive assumptions associated with it, and the myofiber stress predicted by this method can be significantly different from that predicted using a more general FE method [11]. Thus, the FE method should be used to estimate ventricular myofiber stress when available. Such was the case in a study of the Cardiokinetix Parachute device [cite].

In this analysis, the FE method was used to analyze the effects of the Parachute® developed by CardioKinetix Inc (Menlo Park, CA) that is intended to reverse LV remodeling after antero-apical myocardial infarction (MI). This device consists of an expanded polytetrafluoroethylene (ePTFE) membrane bonded to an expanded Nitinol frame consisting of 16 struts. The Nitinol frame is attached to a radioplaque foot. In the deployment process, the device is first collapsed and then delivered percutaneously from the femoral artery by standard catheterization technique. Once in position, the Parachute device is expanded and the anchor tip of each strut engages and hooks on to the LV endocardial wall. In the final deployed configuration, the Parachute device partitions the LV into an upper and a lower chamber (Fig. 2a).

Treatments using this device have shown to lead to a reduction in LV end-diastolic volume (EDV) and end-systolic volume (ESV) in both animals [13] and humans [14] but the mechanism that led to these improvements is unclear. To elucidate its effects, an FE model of the LV implanted with the Parachute® device was constructed. This model is realistic, in particular because 1) the FE LV model was reconstructed from CT images of a patient before Parachute device implantation and 2) the deployment process was simulated in addition to the end-diastole (ED) and ES phases (Fig. 2b).

The main result of this simulation is that treatment using the Parachute device leads to a substantial reduction in ED myofiber stress. The ES myofiber stress, by comparison, was predicted to be a little changed after implantation. Specifically, the average ED myofiber stress was predicted to be 30% lower than that before treatment with the bulk of that reduction coming from the partitioned lower chamber of the LV (Fig. 2c). The results from this single-patient study suggest that the reported therapeutic effects arising from Parachute device treatment may be an outcome of a reduction in ED myofiber stress. Clearly, these results are preliminary and studies involving more patients are required to confirm this result.

3.2 Prediction of pump function

As mentioned earlier, the ability to predict material deformation using the FE method enables it to be used to quantify the ventricular pump function, which is impossible to do so using Laplace's law. This utility was demonstrated in an analysis of the Acorn CorCap Cardiac Support Device (Acorn CSD) using the FE method [15].

The Acorn CSD is a bidirectional woven polyester yarn jacket that is implanted to the epicardial ventricular wall, can be classified under a class of device commonly referred to as a cardiac passive restraint device. Other such devices include the Paracor HeartNet device [16] and the adjustable ventricular restraint device [17]. The primary aim of the restraint device is to reduce elevated ventricular wall stress that is associated with progressive ventricular dilation by mechanically restraining the ventricles. It is hypothesized that doing so will halt or even reverse the adverse ventricular remodeling process.

In this analysis, the mechanical effects of Acorn CSD were simulated using a FE model of a dog biventricular unit with induced dilated cardiomyopathy from rapid pacing (Fig. 3a). We note that a prior FE LV model has also been used to simulate the effects of passive restraint device [18] but that model is highly idealized because it assumed that the LV is a prolate spheroid and the effects of the device is equivalent to that of a constant pressure applied to the epicardium. The biventricular FE model is not restricted by any of these assumptions. In addition, the effects of pre-stretch of the Acorn CSD was also

modeled to address the issue on how tight the Acorn CSD needs to be when it is implanted to the epicardial wall; all that was mentioned in previous studies is that the CSD has to be fitted "snugly" [19].

The results from the simulation show even though the Acorn CSD can reduce the ED myofiber stress substantially (by as large as 78%), and more so with pre-stretch, this huge reduction in myofiber stress was always accompanied by a decrease in diastolic compliance. Consequently, both LV and RV ED pressure-volume relationships were shifted to the left by 7% without pre-stretch and 11% with pre-stretch (Fig. 3b). Because the LV and RV end-systolic pressure-volume relationships were predicted to be insensitive to the presence of Acorn CSD, the Starling's relationship became more depressed and stroke volume was reduced by 23% (without pre-stretch) and 30% (with pre-stretch) as a result (Fig. 3c). Thus, it would be impossible to query the possibility of the Acorn CSD in depressing the ventricular pump function if Laplace's law was used in place of the FE method to evaluate this device.

3.3 Inverse prediction of myocardial material parameters

Because *in vivo* pathological changes of the ventricles are reflected in its regional material properties, the capability to quantify regional ventricular material properties enables one to not only track the evolution of heart diseases but also to quantify the effects of clinical intervention that are intrinsic to the cardiac tissues. The FE method possessed this capability when used in combination with medical imaging techniques capable of measuring *in vivo* myocardial strain, as was demonstrated in a study of the Dor procedure [20].

The Dor procedure (also known as the endoventricular patch plasty procedure) is a surgical procedure used to reduce the LV volume after MI and subsequent LV remodeling. The primary aim of this procedure is to reduce LV wall stress, which is associated to the LV volume according to Laplace's law [21]. It has also been suggested that the Dor procedure may help reduce BZ stress and strain that would improve myocardial contractility at the BZ [22].

To quantify the effects of Dor procedure on regional contractilities and myofiber stress, five MRI-reconstructed FE models of the sheep LV were created at 3 different time points in this study, namely, 2 weeks before surgery, 2 weeks after surgery and 6 weeks after surgery. Based on MR images, the dyskinetic infarct, the BZ and the remote regions were identified and delineated in the LVs as distinct material regions, each with a different contractility reflected by a material parameter of the constitutive law (Fig. 4a). Regional myocardial strain was also measured non-invasively using tagged MRI at these time points. In these FE models, the regional material parameter associated with the tissues contractility were adjusted in a systematic way using computational optimization method so as to minimize the

difference between the FE-predicted and the MR-measured 3-dimensional systolic myocardial strain and the LV cavity volume at ED and ES [23]. Myofiber stress in these sheep models was calculated based on the set of "optimized" material parameters.

Contrary to the hypothesis that BZ contractility would improve after Dor procedure, this study found that the BZ contractility remained depressed when compared to the remote region. Not only did the BZ contractility failed to improve after the Dor procedure, the study also found that the remote region's contractility has decreased by 24% after the procedure (Fig. 4b). On the other hand, myofiber stress at ED and ES were predicted to decrease after the Dor procedure (Fig. 4c). Interestingly, the Surgical Treatment for Ischemic Heart Failure (STICH) trial concluded that adding the Dor procedure to coronary artery bypass grafting adds no benefits to the patient [24] even though that result is controversial and other clinical studies have found that such a procedure can benefit patients [25]. Given that there are other kinds of variants of the Dor procedure (e.g. the Pacopexy technique [26]), computational modeling, as shown in this study, can be both useful and efficient in providing an insight to the regional pathological changes of the ventricles associated with such procedures.

3.4 Simulation of surgery

Because of its versatility, the FE method can be used to simulate surgery and hence, can potentially be used for surgery planning. The key to this potentiality lies in the method's ability to simulate the suturing process, as was demonstrated in our two recent analyses of mitral annuloplasty [26, 27].

Though FE modeling has been used extensively to model mitral regurgitation (e.g. [29]) and the effects of the mitral annuloplasty using different type of rings (e.g. [30–32]), the mitral valve apparatus is usually isolated from the LV and studied individually. Recently, our group created the first FE model of the mitral valve incorporated into an animal-specific infarcted LV [11]. This model contains most of the structural components found in a complete LV-mitral-valve assembly. Specifically, the model contains the mitral valve leaflets, the chordae tendinae, the papillary muscles and the LV, which are all connected to one another in an anatomically realistic fashion (Fig. 5a). Building upon this model, Wong et al. [28] investigated the effects of mitral annuloplasty shape in ischemic mitral regurgitation by virtually suturing two different shaped mitral annuloplasty rings, namely, a saddle-shape and an asymmetric-shape (Fig. 5b), to the mitral annulus of the model. The virtual sutures were modeled using two-node "beam" elements with one end attached to the annuloplasty ring and the other attached to the mitral annulus (Fig. 5c). An axial tension was then prescribed in each "suture" element so that its two ends were "pulled" towards each other. As a result, the mitral annulus was pulled towards the annuloplasty ring until the annulus conformed to the ring shape.

Besides the principal findings of this study: that the effects of mitral annuloplasty are generally insensitive to the shape of annuloplasty ring such that both septolateral distance and coaptation of the mitral leaflets were improved with implantation of these two types of annuloplasty rings (Fig. 5d), the modeling of sutures as described in this study should in principle also enable the FE method to be used for planning and/or optimizing of other cardiac surgical procedures.

4. Conclusion

Using various examples, we have demonstrated four specific capabilities of computational cardiac modeling, namely, its ability to simulate surgery, predict myofiber stress and pump function, and quantify changes to myocardial material properties. In this review, we have offered only a glimpse of the potentially huge role that computational modeling can play in cardiac surgery. We foresee that in time, computational modeling will become an indispensable tool in accelerating the development of effective medical treatments and in improving patient care. Perhaps one day, patient-specific computational modeling may even form the basis for clinical decision making.

Several issues would need to be resolved in order for computational modeling to play a greater role in cardiac surgery, especially in patient-specific computational modeling. First, the construction of patient-specific FE model is generally time-consuming and requires laborious steps. This is especially so given the current lack of automatic segmentation tools to reconstruct ventricular geometry from medical images that is suitable for FE modeling. Second, current constitutive laws of cardiac tissues were formulated mostly based on *ex vivo* experimental tests and may not reflect all the properties encapsulated *in vivo*. For example, no constitutive law describing the growth in living cardiac tissues have been rigorously validated experimentally (though several such laws have been proposed). Thus, current computational model can only be suitably applied to study the acute effects of diseases and clinical interventions. Third, microstructure of the cardiac tissues (e.g. myofiber orientation in the ventricular walls) is only known grossly in the explanted heart via invasive histological measurements or non-invasive diffusion tensor imaging. As such, current patient-specific ventricular models are only "geometrically" patient-specific, and by no means are "microstructurally" patient-specific. It is only very recently that *in vivo* measurement of myofiber orientation with diffusion tensor imaging becomes possible although the total scan time of 10 – 15 minutes per image slice [33] may still be challenging for heart failure patients. All in all, the issues mentioned here are not exhaustive but nonetheless, the future of computational modeling in cardiac surgery remains bright with huge potential to be reaped.

5. Acknowledgments

This study was supported by NIH grants R01-HL-084431 (Dr. Ratcliffe); R01-HL-077921 and R01-HL-086400 (Dr. Guccione); and by a Marie-Curie international outgoing fellowship within the 7th European Community Framework Programme (Dr. Genet).

6. References

[1] YC F. Stress, strain, growth, and remodeling of living organisms. *Z. Angew. Math. Phys.* 1995; S469–82

[2] Humphrey JD. Review Paper: Continuum biomechanics of soft biological tissues. *Proc R Soc A* 2003; 459:3–46

[3] Janz RF, Grimm a. F. Finite-Element Model for the Mechanical Behavior of the Left Ventricle: Prediction of Deformation in the Potassium-arrested Rat Heart. *Circ Res* 1972; 30:244–252

[4] Wall ST, Guccione JM, Ratcliffe MB, Sundnes JS. Electromechanical feedback with reduced cellular connectivity alters electrical activity in an infarct injured left ventricle: a finite element model study. *Am J Physiol Heart Circ Physiol* 2012; 302:H206–14

[5] Guccione JM, Kassab GS, Ratcliffe MB. Computational Cardiovascular Mechanics. 2010;

[6] Fung Y. A first course in continuum mechanics. 1977;

[7] Guccione JM, Waldman LK, McCulloch AD. Mechanics of active contraction in cardiac muscle: part II-cylindrical models of the systolic left ventricle. *J. Biomech. Eng.* 1993; 115:82–90

[8] Guccione JM, Costa KD, McCulloch AD. Finite element stress analysis of left ventricular mechanics in the beating dog heart. *J. Biomechanics* 1995; 28:1167–1177

[9] Yin FC. Ventricular wall stress. *Circ Res* 1981; 49:829–842

[10] Streeter DD, Spotnitz HM, Patel DP, Ross J, et al. Fiber orientation in the canine left ventricle during diastole and systole. *Circ. Res.* 1969; 24:339–47

[11] Zhang Z, Tendulkar A, Sun K, Saloner D a, et al. Comparison of the Young-Laplace law and finite element based calculation of ventricular wall stress: implications for postinfarct and surgical ventricular remodeling. *Ann Thorac Surg* 2011; 91:150–6

[12] Grossman W. Cardiac hypertrophy: useful adaptation or pathologic process? *Am. J. Med.* 1980; 69:576–584

[13] Nikolic SD, Khairkhahan A, Ryu M, Champsaur G, et al. Percutaneous implantation of an intraventricular device for the treatment of heart failure: experimental results and proof of concept. *J. Card. Fail.* 2009; 15:790–7

[14] Sagic D, Otasevic P, Sievert H, Elsasser A, et al. Percutaneous implantation of the left ventricular partitioning device for chronic heart failure: a pilot study with 1-year follow-up. *Eur. J. Heart Fail.* 2010; 12:600–6

[15] Wenk JF, Ge L, Zhang Z, Mojsejenko D, et al. Biventricular Finite Element Modeling of the Acorn CorCap Cardiac Support Device on a Failing Heart. *Ann Thorac Surg* 2013; 95:2022–7

[16] Magovern J a. Experimental and clinical studies with the Paracor cardiac restraint device. *Semin Thorac Cardiovasc Surg* 2005; 17:364–8

[17] Ghanta RK, Rangaraj A, Umakanthan R, Lee L, et al. Adjustable, physiological ventricular restraint improves left ventricular mechanics and reduces dilatation in an ovine model of chronic heart failure. *Circulation* 2007; 115:1201–10

[18] Jhun CS, Wenk JF, Zhang Z, Wall ST, et al. Effect of adjustable passive constraint on the failing left ventricle: A finite element model study. *Ann. Thorac. Surg.* 2010; 89:132–137

[19] Oz MC, Konertz WF, Kleber FX, Mohr FW, et al. Global surgical experience with the Acorn cardiac support device. *J Thorac Cardiovasc Surg* 2003; 126:983–991

[20] Sun K, Zhang Z, Suzuki T, Wenk JF, et al. Dor procedure for dyskinetic anteroapical myocardial infarction fails to improve contractility in the border zone. *J Thorac Cardiovasc Surg* 2010; 140:233–9, 239.e1–4

[21] Menicanti L, Di Donato M. The Dor procedure: What has changed after fifteen years of clinical practice? *J Thorac Cardiovasc Surg* 2002; 124:886–890

[22] Ratcliffe MB. Non-Ischemic Infarct Extension: A New Type of Infarct Enlargement and a Potential Therapeutic Target. *J Am Coll Cardiol* 2002; 40:1168–1171

[23] Sun K, Stander N, Jhun C-S, Zhang Z, et al. A computationally efficient formal optimization of regional myocardial contractility in a sheep with left ventricular aneurysm. *J. Biomech. Eng.* 2009; 131:111001

[24] Jones RH, Velazquez EJ, Michler RE, Sopko G, et al. Coronary Bypass Surgery with or without Surgical Ventricular Reconstruction. *New Engl J Med* 2009; 360:1705–1717

[25] Buckberg G, Athanasuleas C, Conte J. Surgical ventricular restoration for the treatment of heart failure. *Nat Rev Cardiol* 2012; 9:703–16

[26] Isomura T, Horii T, Suma H, Buckberg GD. Septal anterior ventricular exclusion operation (Pacopexy) for ischemic dilated cardiomyopathy: treat form not disease. *Eur J Cardiothorac Surg* 2006; 29 Suppl 1:S245–50

[27] Wenk JF, Zhang Z, Cheng G, Malhotra D, et al. First finite element model of the left ventricle with mitral valve: insights into ischemic mitral regurgitation. *Ann Thorac Surg* 2010; 89:1546–53

[28] Wong VM, Wenk JF, Zhang Z, Cheng G, et al. The effect of mitral annuloplasty shape in ischemic mitral regurgitation: a finite element simulation. *Ann Thorac Surg* 2012; 93:776–82

[29] Kunzelman KS, Reimink MS, Cochran RP. Annular dilatation increases stress in the mitral valve and delays coaptation: a finite element computer model. *Cardiovasc Surg* 1997; 5:427–434

[30] Kunzelman KS, Reimink MS, Cochran RP. Flexible versus rigid ring annuloplasty for mitral valve annular dilatation: a finite element model. *J Heart Valve Dis* 1998; 7:108–116

[31] Votta E, Maisano F, Bolling SF, Alfieri O, et al. The Geoform disease-specific annuloplasty system: a finite element study. *Ann Thorac Surg* 2007; 84:92–101

[32] Rausch MK, Bothe W, Kvitting J-PE, Swanson JC, et al. Mitral valve annuloplasty: a quantitative clinical and mechanical comparison of different annuloplasty devices. *Ann Biomed Eng* 2012; 40:750–61

[33] Toussaint N, Stoeck CT, Sermesant M, Schaeffter T, et al. In vivo human cardiac fibre architecture estimation using shape-based diffusion tensor processing. *Med Image Anal* 2013;

7. Figures

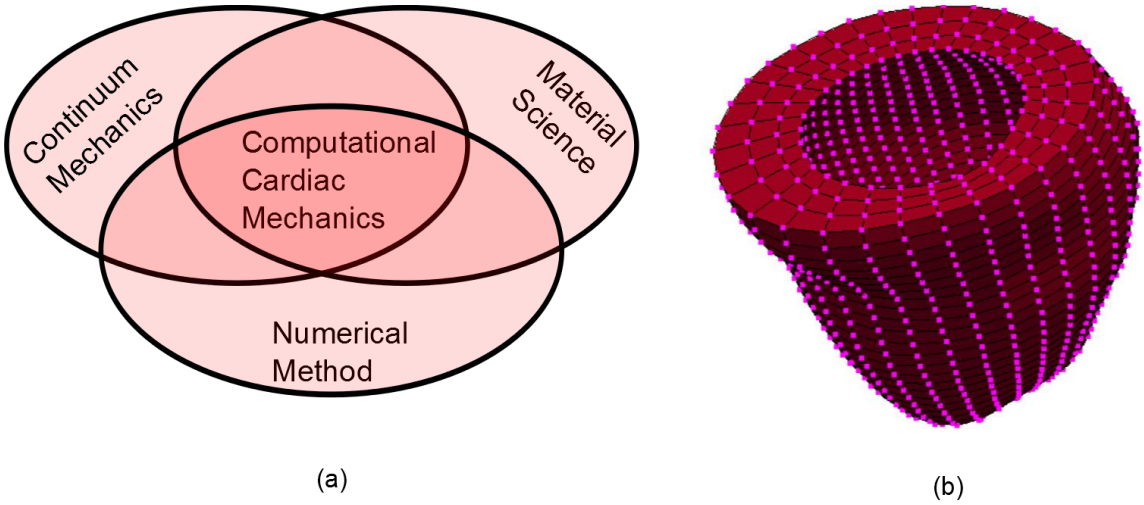

Figure 1(a): Computational cardiac mechanics as an intersection of three domains: continuum mechanics, material science and numerical method. **(b):** A FE mesh of a LV. The elements (demarcated by the black lines) are inter-connected through nodes (shown in pink).

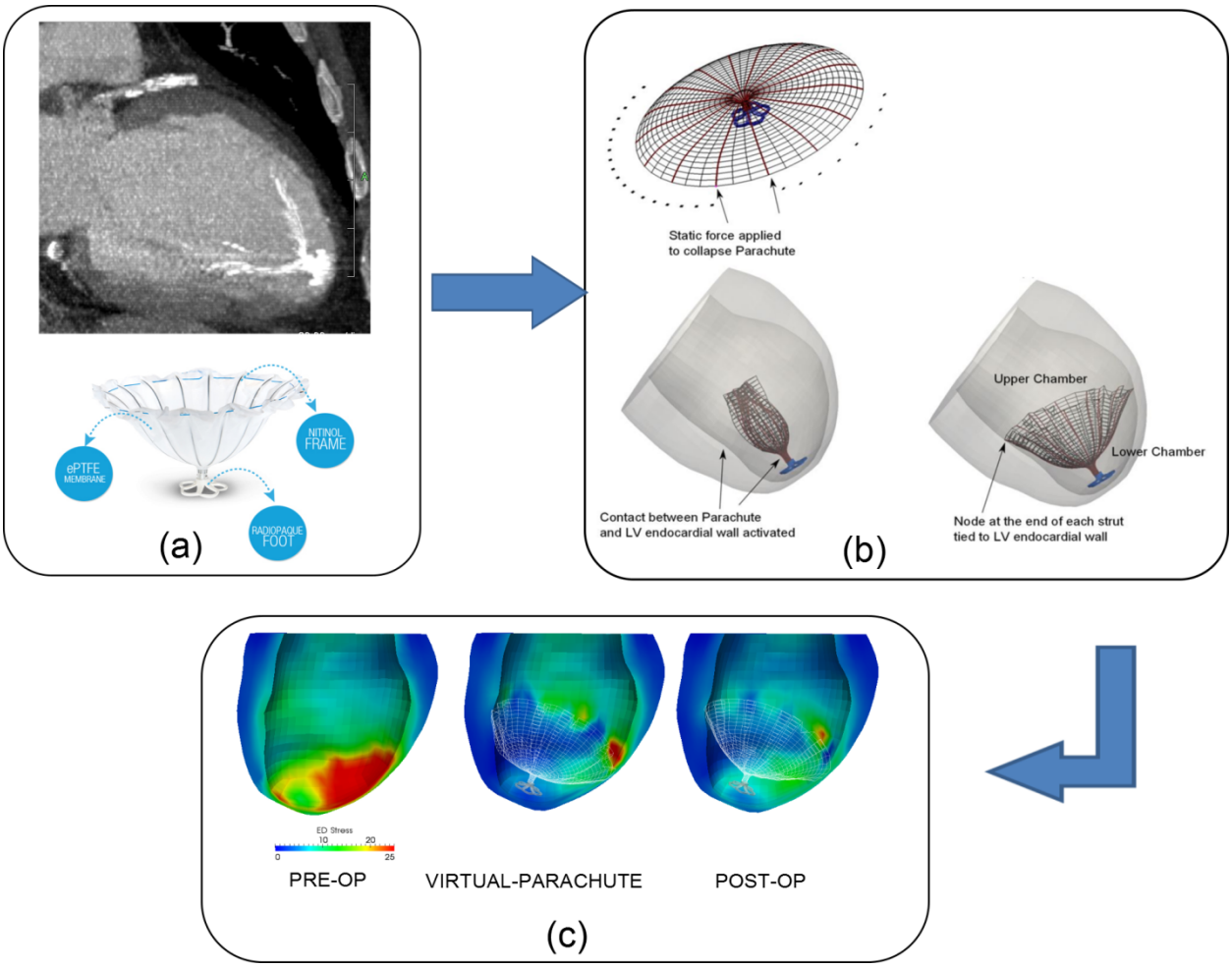

Figure 2: Simulation of the Cardiokinetix Parachute Device. (a) Upper: CT image of the Parachute device implanted in a patient. Lower: the Parachute device. (b) Simulating the deployment of the Parachute device in the FE model. (c) Comparison of the LV myofiber stress distribution at ED before and after treatment.

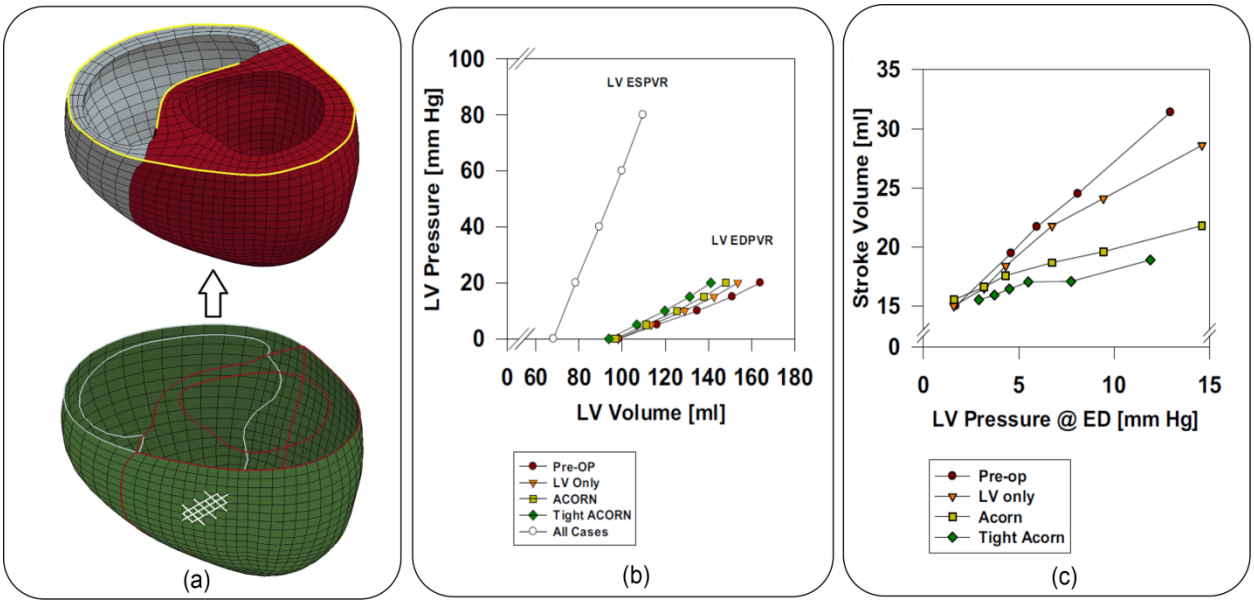

Figure 3: Simulation of the Acorn CorCap CSD. (a) Upper: biventricular FE model showing the LV in red and right ventricle in grey. Lower: CSD model before attachment to the biventricular model as outlined by the red and gray lines. Criss-cross white lines indicate the CSD fiber orientations. (b) Effects of CSD on ED and ES pressure-volume relationships. (c) Effects of CSD on Starling's relationships. "Tight ACORN" refers to the case when a 5% pre-stretch was applied to the CSD and "LV-Only" refers to the case when the CSD encircles only the LV.

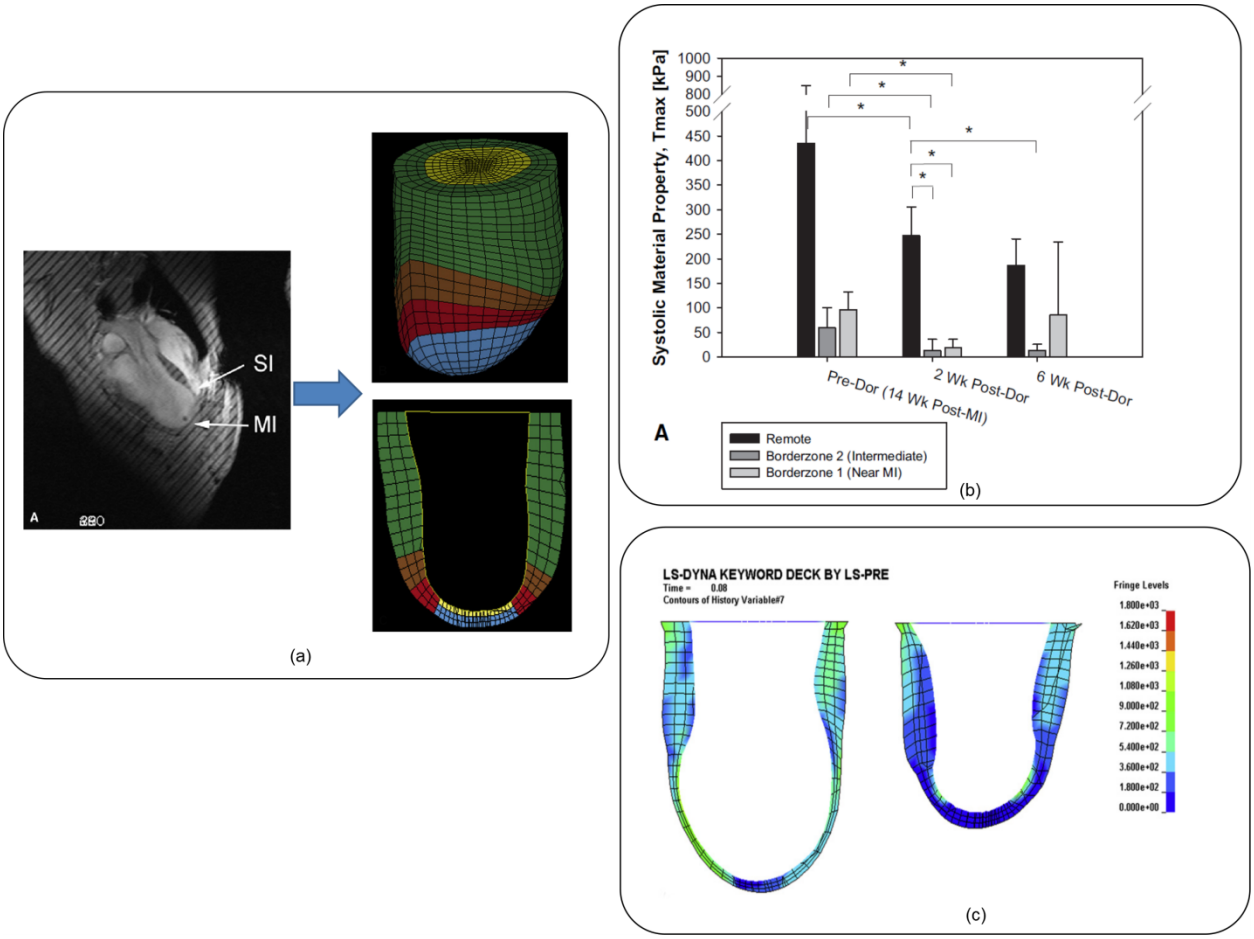

Figure 4: Simulation of the Dor procedure. (a) Left: magnetic resonance image showing the long-axis view of the sheep LV after MI. MI and SI denote the dyskinetic and septal infarct, respectively. Tagged lines used to compute the myocardial strain can also be seen in the image. Top right: FE model of the LV. Bottom right: view of a cross section slice of the FE model. Blue, red, brown and green regions denote the infarct, the BZ 1, BZ 2 and the remote region, respectively. (b) Effects of Dor procedure on the regional myocardial contractility as reflected by the systolic material parameter. (c) Effect of Dor procedure on the longitudinal and transmural distributions of end-systolic myofiberstress pre-Dor (left) and 6weeks post-Dor (right) in a typical sheep. Fringe level units in hPa.

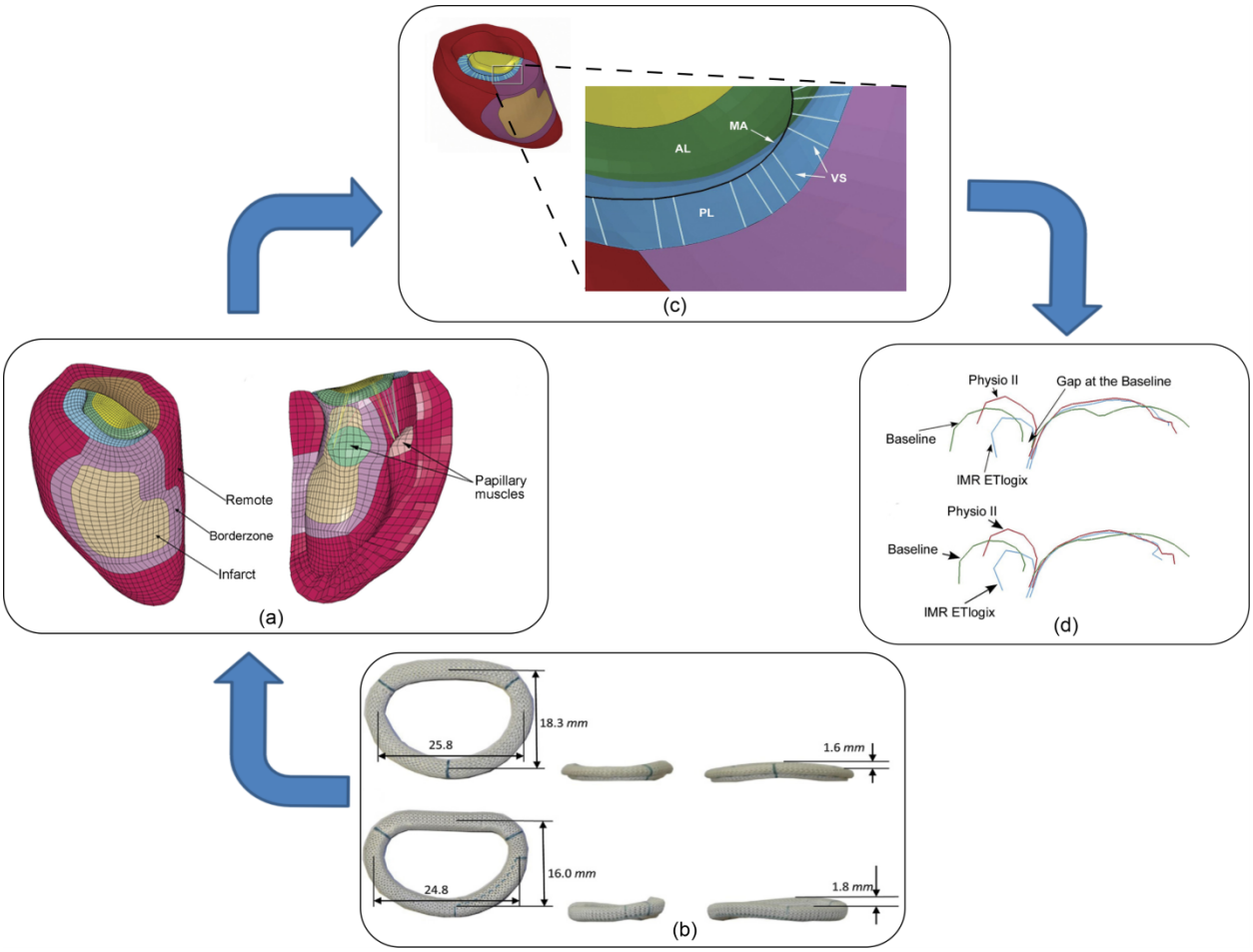

Figure 5: Simulation of mitral valve annuloplasty. (a) FE model of the LV with the mitral valve apparatus i.e. mitral valve leaflets, chordae tendinae and the papillary muscle. (b) Annuloplasty rings with different shapes (from Edward Lifesciences, Inc, Irvine, CA). Top: saddle shape ring (Physio II). Bottom: asymmetric ring (IIMR ETlogix). (c): Annuloplasty ring virtually sutured to the mitral annulus (MA). Tension is imposed in the virtual suture (VS, shown here without tension) so that MA is pulled towards annuloplasty ring (AL = anterior leaflet, PL = posterior leaflet). (d): Improvement of the mitral leaflet coaptation after mitral annuloplasty.

Appendix: A simplified description of the finite element method

As discussed in the main text, computational cardiac mechanics is at the intersection of three scientific domains, namely, continuum mechanics, materials science and numerical methods. Here, we use a simple one-dimensional linear and static example problem to illustrate these three intersecting domains, as well as key aspects of the finite element method. For more detailed formulations, please refer to [A1].

Consider the following problem in which we want to determine the equilibrium state of a long and slender structure (e.g. a leg bone) under the influence of body force (e.g. gravity) and contact forces (e.g. from adjacent bones). To simplify this problem, we idealize the slender structure as a one-dimensional system represented in Figure A1.

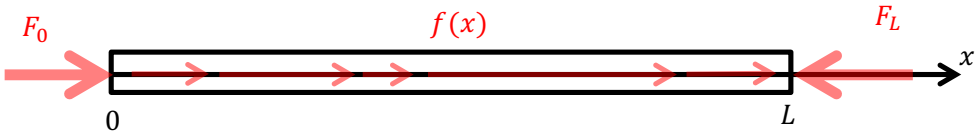

Figure A1. Idealization of the studied slender structure as a one-dimensional medium, with body force $f(x)$ and contact forces F_0 and F_L

We consider the axial displacement u at every point of the structure defined by the point location x as unknown. In other words, we seek a solution for the unknown function $u(x)$ (or u as a function of x) that is defined over the length of the structure from $x = 0$ to $x = L$.

Continuum Mechanics

The foundation of continuum mechanics lies in its three conservation principles, namely, conservation of mass, momentum and energy. Since the system considered here is closed i.e. there is no mass transfer, conservation of mass is satisfied trivially. Also, since we are not considering any other kind of energy (e.g. heat energy, chemical energy) besides mechanical energy, the conservation of energy does not add anything to the conservation of momentum. Thus the only relevant conservation principle in this problem is the conservation of momentum, which is expressed as follows:

$$\frac{d\sigma}{dx} + f(x) = 0\,, \tag{1}$$

where σ is the axial stress inside the beam (i.e. the axial stress that neighboring sections impose on each other, in N/m^2 or Pa), and f is the body force (in N/m^3). Note that for the sake of simplicity, we assume that the beam section is constant and is equal to 1. Basically, Equation (1) describes the (point-wise) internal equilibrium of the structure; it essentially means that the body force induce a change in stress

within the structure. The external equilibrium of the structure is imposed by the following 2 equations called boundary conditions:

$$\begin{cases} \sigma(0) = F_0 \\ \sigma(L) = F_L \end{cases}, \tag{2}$$

where F_0 & F_L are the contact forces. These equations essentially means that the axial stress at both ends of the structure must be equal to the contact force imposed at that particular end.

Material Science

As explained Section 2.1, the continuum mechanics principles discussed above are completely general, and applies to all types of materials. The different mechanical behavior exhibited by different materials is distinguished by a material or constitutive law that is specific to the material. The simplest possible material law is one in which the stress σ is proportional to the strain with a constant of proportionality E called the Young's Modulus i.e.

$$\sigma = E\frac{du}{dx}. \tag{3}$$

In Equation (3), the strain is given by $\frac{du}{dx}$, which is essentially the ratio between a change in length and the original length taken point-wise in the structure. Of course, cardiac tissue has more complex mechanical behavior and its constitutive laws are therefore more complex than the one described here. For example, stress is a non-linear function of strain in cardiac tissues.

Numerical Methods

Now, the goal is to find a function for the axial displacement $u(x)$ that satisfies Equations (1) – (3). However, it is often difficult to find such a function that can be expressed in analytical form in problems involving realistic geometry and complex material behavior (though not in this example). Hence, numerical methods that can be implemented easily using computers are often used to find an approximate solution. Because of its versatility, the finite element method is often used to find an approximate solution for complex problems.

Equations (1) & (2) are local or point-wise expressions of equilibrium principles, often called the strong form. To make the solution tractable, the finite element method splits the original continuous problem into a discrete one in a process typically known as "discretization". To do so, these 2 equations must be expressed in a global form, often called the weak form:

$$\int_0^L \frac{d\delta u}{dx}\sigma(x)dx = \int_0^L \delta u(x)\, f(x)dx + \delta u(0)F_0 + \delta u(L)F_L\,, \tag{4}$$

where δu defines a virtual axial displacement field, a concept that will be described later. It is important to say that the weak and strong formulations are strictly equivalent, and they can be transformed from one to the other. The weak formulation is also called the variational formulation and it is essentially due to Galerkin. As an aside, the finite element method is also often called the Ritz-Galerkin method to reflect the contribution of Ritz to this method.

Equation (4) is sometimes introduced directly in lieu of the conservation equations (1) & (2) by invoking the principle of virtual work. This principle has a clear physical meaning: every term is either a product between stress and strain (term in LHS) or between displacement and force (terms in RHS) and is therefore a mechanical work or mechanical energy. In other words, Equation (4) means that for every virtual axial displacement field, the virtual work due to internal forces (i.e. stresses) must be equal to the virtual work due to the imposed forces (i.e. the body force and the contact forces in this example).

Substituting Equation (3) into (4), we obtain a variational equation containing the equations originating from continuum mechanics and material science discussed until now:

$$\int_0^L E \frac{d\delta u}{dx} \frac{du}{dx} dx = \int_0^L \delta u(x) f(x) dx + \delta u(0) F_0 + \delta u(L) F_L \; \forall \delta u \,, \tag{5}$$

We are now ready to discretize Equation (5) using the finite element method. Following Ritz method, the approximated solution $u^h(x)$ to Equation (5) is expressed as a weighted sum or linear combination of known functions often called shape functions $\varphi_i(x)$:

$$u^h(x) = \sum_i u_i \varphi_i(x) \,, \tag{6}$$

where u_i are the unknown coefficients to be determined from the finite element problem. Thus, instead of seeking an exact solution for the axial displacement $u(x)$ that is smooth or continuous in the structure, we are now seeking an approximated solution $u^h(x)$ (generated by a finite number of shape functions) that is not as smooth as the exact solution.

The definition of shape functions is key to the finite element method. These functions are defined in such a way that the structure can be divided into many simple parts called elements, whose vertices are called nodes. The resultant computational geometry obtained after discretization (i.e. after the assembly of nodes and elements) is called a finite element mesh. For simple geometries, generating the computational geometry can be fast and automatic but for complex geometries, this process can be extremely time-consuming.

For our simple problem, the structure is divided into several sub-segments (say $N-1$ segments with N nodes). Also, we consider a family of piecewise linear shape functions such that (i) there is one shape

function associated with each node; and (ii) each shape function equals 1 on its node and 0 on all other nodes as shown below. By this definition, the unknown coefficients u_i are the axial displacement at each node.

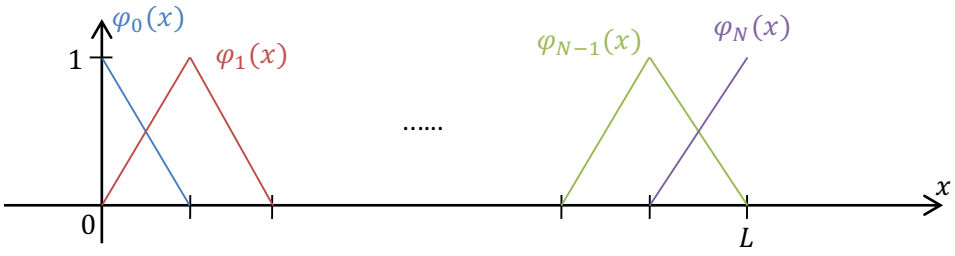

Figure A2. Family of piecewise linear shape functions

In the above figure, one can see that by adjusting the weights associated with each shape function, this family of shape functions can generate every piecewise linear function over the structure. More complicated shape functions such as quadratic shape functions can also be used.

Substituting Equation (6) into the weak formulation in Equation (5), we obtain:

$$\int_0^L E \sum_j \delta u_j \varphi_{j,x}(x) \sum_i u_i \varphi_{i,x}(x)\, dx = \int_0^L \sum_i \delta u_i \varphi_i(x)\, f(x) dx + \delta u_0 F_0 + \delta u_N F_L \;\forall \delta u_i \tag{7}$$

Note that the same discretization has been applied to the unknown displacement function u and the virtual displacement δu leading to a symmetric LHS (i.e that term does not change if we switch the subscript i with j or vice-versa. Equation (7) can be written in algebraic or matrix form

$$\underline{\delta U}^T \underline{K}\, \underline{U} = \underline{\delta U}^T \underline{F}\,, \tag{8}$$

which is equivalent to

$$\underline{K}\, \underline{U} = \underline{F}\,. \tag{9}$$

In Equation (9), $K_{ij} = \int_0^L E \varphi_{i,x}(x) \varphi_{j,x}(x)\, dx$ is called the stiffness matrix that contains information on the stiffness of each part of the system and $F_j = \int_0^L \varphi_j(x)\, f(x) dx + \delta_{0j} F_0 + \delta_{Nj} F_L$ is called the force vector that contains information on the loading on each part of the system. The solution of the finite element problem $\underline{U}$ (a vector containing the axial displacement at each node u_i) is usually computed by solving the linear system (9) with computers.

Once the linear system is solved, the approximated piecewise linear solution can be constructed using Equation (6). The approximated solution $u^h(x)$ is shown in Figure A3 for the case without contact forces but with body force $f(x) = \sin(x)$. In that same figure, we also show the exact solution, which can be expressed analytically for this simple problem though this is usually not the case in more complicated problems.

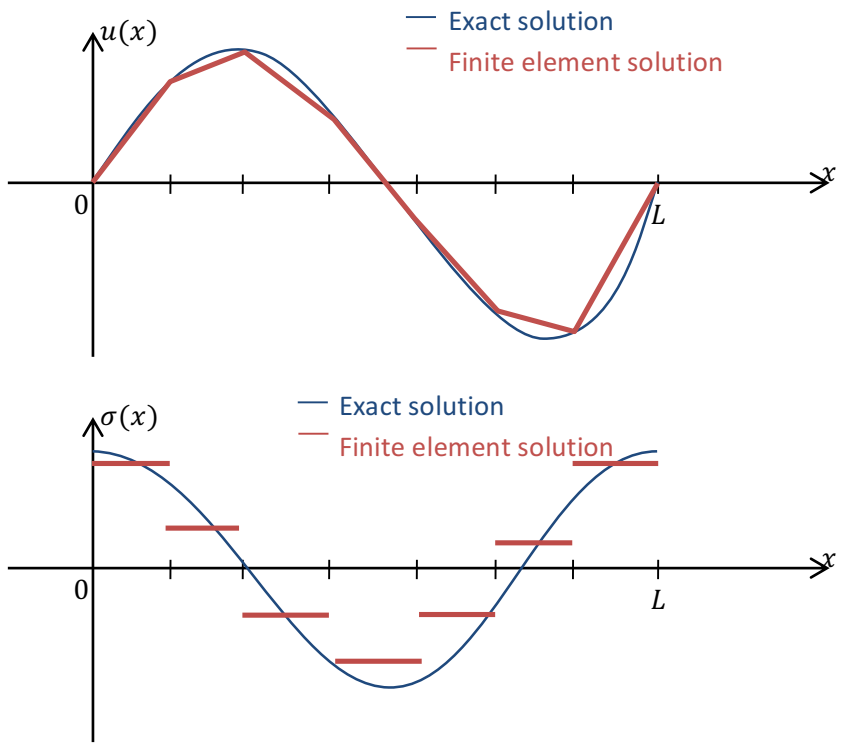

Figure A3. Finite element solution of the problem compared to the exact solution

One can make a few observations concerning the finite element solution in Figure A3. First, it is evident that the finite element solution is piecewise linear and is therefore, not as smooth as the exact solution. However, the approximate solution will approach the exact solution as the mesh is made finer with more elements and nodes. Second, the stress computed by the finite element method σ is constant within elements and is discontinuous across elements (also true for strains). Thus, they are not "well" defined at the nodes. This result is largely due to our choice of the shape functions which produced piecewise linear solution.

References

[1] T. Belytschko, W. K. Liu, and B. Moran, *Nonlinear Finite Elements for Continua and Structures*. Wiley, 2002.